Automated Detection of 3D Landmarks for the Elimination of Non-Biological Variation in Geometric Morphometric Analyses

D Aneja[1], SR Vora[2,5], ED Camci[2,5], LG Shapiro[1] and TC Cox[3,4,5]

[1]Department of Computer Science, University of Washington, Seattle, WA
[2]Department of Oral Health Sciences, University of Washington, Seattle, WA
[3]Department of Pediatrics, University of Washington, Seattle, WA
[4]Department of Anatomy & Developmental Biology, Monash University, Clayton, Victoria, Australia
[5]Center for Developmental Biology & Regenerative Med., Seattle Children's Research Institute, Seattle, WA
Email : {deepalia, shapiro}@cs.washington.edu, {svora, ecamci, tccox}@uw.edu

Abstract—**Landmark-based morphometric analyses are used by anthropologists, developmental and evolutionary biologists to understand shape and size differences (eg. in the cranioskeleton) between groups of specimens. The standard, labor intensive approach is for researchers to manually place landmarks on 3D image datasets. As landmark recognition is subject to inaccuracies of human perception, digitization of landmark coordinates is typically repeated (often by more than one person) and the mean coordinates are used. In an attempt to improve efficiency and reproducibility between researchers, we have developed an algorithm to locate landmarks on CT mouse hemi-mandible data. The method is evaluated on 3D meshes of 28-day old mice, and results compared to landmarks manually identified by experts. Quantitative shape comparison between two inbred mouse strains demonstrate that data obtained using our algorithm also has enhanced statistical power when compared to data obtained by manual landmarking.**

I. INTRODUCTION

Analysis of morphological variation requires quantifying changes in size and shape. Of these, size changes are relatively easy to measure whereas quantifying shape variation can be challenging, especially when differences are subtle. Geometric morphometrics encompasses a category of analytic techniques aimed at studying shape variation between groups or organisms, differing in either phylogeny or ontogeny. Traditional morphometric methods are based on acquiring 2- or 3- dimensional representation of specimens followed by manual annotation of landmarks corresponding to anatomical structures of interest. These landmarks are then used to obtain linear measurements, angular measurements, derived measurements such as ratios between inter-landmark distances, or principal components of differences from overall landmark configurations. Such methods have been instrumental in studying craniofacial morphology by various fields including evolutionary and developmental biology, anthropology, pediatric orthopedics, orthodontics and forensic sciences. Coupled with other data, morphometrics is useful for investigating specific contributions of genetic, epigenitic, ecological and environmental factors on normal craniofacial growth and dysmorphology.

Advances in 3-dimensional computer-aided tomographic image acquisition (3D CT) as well as visualization and analytic software, coupled with enhanced GPU-based data processing, have greatly aided morphometric techniques. Nevertheless, manual placement of multiple points on 3D renderings or meshes derived from CT-scans can be exceptionally labor intensive, and require training investigators on precise identification of points. This introduces inter- and intra-investigator variability, which can impact quantitative comparisons by potentially obscuring subtle, yet significant biological differences between groups. Methods that reduce this variability can vastly improve the statistical power of performed analyses and decrease the chances of Type II errors (i.e. incorrectly accepting the null hypothesis of no difference), without the need to dramatically increase sample size.

In this paper, we present an algorithm-based system to automatically detect 17 landmarks on 3D meshes of mouse mandibles, based entirely upon mathematically defined criteria. This automated method is compared to the traditional method of manual landmarking, with obtained inter and intra-investigator measurement variability. Traditional, Procrustes based shape analyses are also performed to compare landmarks from manual and automated datasets, to validate the accuracy of our technique.

II. RELATED WORK

Automated landmarking of 3dMD datasets has been attempted by a few groups [1], [2] and improved upon by using deformable registration [3]. Nowinski *et.al.* [4] utilized 3D magnetic resonance volumetric neuroimages to localize landmarks (curvature extrema, inter-sectional and terminal) using a semi-global segmentation and point-anchored registration approach. Tautz et. al.[5] describe a semi-automated approach to landmark a query image that relies on the presence of a manually annotated training set. Limited user input is required to first identify four landmarks, following which, the query image is registered to the training image using a hierarchical

multi-stage patch-based approach. Each image in the training set yields an estimated location of a landmark, from which a final estimate is output utilizing an array-based voting system. This method demonstrated comparable accuracy with improved repeatability over the traditional, manual annotation method.

III. DATA AND PREPROCESSING

Two highly inbred wildtype strains were used in this study; C57BL/6 mice and AJ(stock #000664 and #000646; Jackson Laboratories, ME). Littermates of each strain can be considered genetically identical and thus phenotypic variability can be attributed to epigenetic effects and/or somatic genetic changes. To eliminate differences due to sexual dimorphism, only male mice were used for the analyses. The mice were bred in a controlled environment at Seattle Children's Research Institute (Seattle, WA) and euthanized by CO_2 inhalation at postnatal day 28 (∼1 month of age). Crania were imaged using a Skyscan 1076 micro Computed Tomography (microCT) scanner at $35\,\mu m$ and all data reconstructed using consistent parameters. Because of its relatively simple shape, the mandible has long been the focus of morphometric studies and was chosen as a starting point to validate our methodology. Moreover, the two halves of the mouse mandible (hemi-mandibles) are symmetrically positioned about the midline and are readily segmented (either in a unit or as hemi-mandibles) from the rest of the craniofacial skeleton in CT data. Segmentation was performed and a surface mesh with ∼17K points generated for each scan using Analyze 10.0 (Mayo Clinic, Rochester, MN) utilizing the Adaptive Deformation algorithm. Rapidform XOR (INUS Technology) was used to mirror the left hemi-mandible surfaces to the right hemi-mandible conformation. A total of 14 individual C57BL/6J and 10 AJ mice were used to obtain the samples for our study.

Morphometric studies have broadly classified landmarks as either Biological, Constructed, or Fuzzy [6], [7]. *Biological* landmarks (Type-B) are based purely on anatomic features and can be identified independent of orientation. *Constructed* landmarks (Type-C) are determined by constructing a line tangent to other structures or bony edges and hence, are dependent on appropriate orientation of the rendering. Several landmarks are considered *Fuzzy* (Type-F), in that their definitions encompass areas larger than a single point within the investigators range of view. We used a total of 17 landmarks which encompass all types of points (B, C and F) following the standard definition as described in Table I and illustrated in a schematic shown in Fig.1.

IV. METHODOLOGY

A. Manual Landmarking

Landmarking was performed manually on the 3D surface mesh files using IDAV Landmark (UC Davis). Each of the C57BL/6J hemi-mandible was manually landmarked 3 times by one investigator. The Euclidean distance between two points that represent the same landmark at separate instances was measured as intra-investigator error. Hence each C57BL/6J hemi-mandible provided three such distances which were analyzed over all the 28 hemi-mandible dataset, to compute intra-investigator variability (precision) for each landmark. Two additional investigators manually marked the points for C57BL/6J dataset, for the purpose of calculating inter-investigator variability. In this instance, the Euclidean distance between the points that were deemed to represent the same landmark by the three investigators represented inter-investigator error. The dataset comprised of AJ hemi-mandible was manually landmarked by one investigator. All investigators were trained to identify the landmarks with the standard definitions (Table I and Fig.1) and worked independent of one another.

B. Automated Landmarking

The automated landmarking method detects 17 landmarks on the 3D mesh surface of mouse hemi-mandible data. The initial orientation views the right hemi-mandible from the medial surface (the surface naturally facing the midline of the animal) with the incisor pointing to the left (anterior) and the condylar process pointing superiorly to the right (posterior)
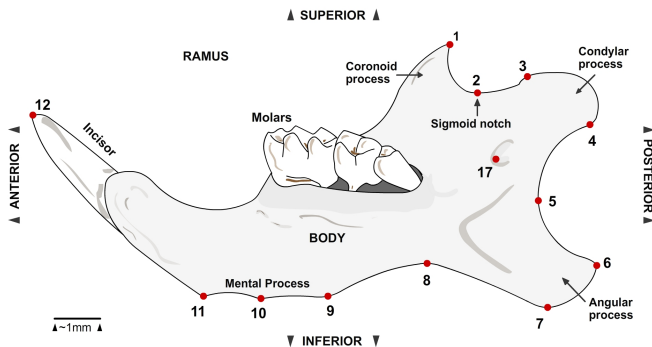

Fig. 1. Schematic of the medial surface of the right mandible showing landmarks used in this study. (Note $LM14$, $LM15$ and $LM16$ are not seen in this view).

TABLE I
DEFINITION OF LANDMARKS IDENTIFIED IN THIS STUDY CATEGORIZED AS BIOLOGICAL (B), FUZZY (F) AND CONSTRUCTED (C).

LM	Abbr	Description	Type
1	cor	Most prominent point on the tip of coronoid process	B
2	sgn	Deepest (anteor-inferior) point on sigmoid notch	C
3	cda	Most antero-superior point on condylar process	F
4	cdi	Most postero-inferior point on condylar process	F
5	pra	Deepest point on posterior border of ramus	C
6	g	Most prominent point on tip of angular process	B
7	iap	Most prominent point on inferior margin of angular process	C
8	mpp	Deepest point on inferior border of the ramus	C
9	gn	Most prominent postero-inferior point on mental process	F
10	mmp	Most prominent point on middle protusion of mental process	F
11	m	Most prominent antero-inferior point on mental process	F
12	lit	Tip of manidbular incisor	B
13	lil	Midpoint on alveolar ridge lingual to incisor	F
14	men	Deepest point on posterior margin of mental foramen	B
15	mtr	Masseteric tubercle	F
16	urm	Intersection of coronoid process and body of mandible	F
17	lig	Deepest point on anterior margin of lingual foramen	B

as shown in Fig. 1. In this orientation, the most prominent anterior point on the inferior surface of the mental process points downward. Our geometric detection method is initially used to normalize the surface meshes. This alignment aids in detecting constructed landmarks, which require a defined orientation for standardized recognition.

Our method requires the surface mesh of the mandible to be normalized such that antero-posterior dimension is along the x-axis, supero-inferior dimension is along the y-axis and medio-lateral dimension is along the z-axis as shown in Fig. 1. This requires manual input from the user, with an accuracy range of $\sim$12 degrees in any direction. Since the definitions of Biological and Fuzzy landmarks are locally defined, they are essentially independent of image orientation. However, constructed points are dependent entirely on orientation of user view. The mesh is oriented by applying an affine transformation to the projection matrix such that the projection of the Euclidean distance between points $LM6$ and $LM11$ was maximal with respect to the world view, defining orientation around the y-axis. To define the rotation around the z-axis, the line $LM6$-$LM11$ was made parallel to the x-axis. Finally, the mesh was rotated around the x-axis such that the projection of the euclidean distance between points $LM6$ and $LM1$ was maximal with respect to the world view.

Data bounds are calculated in the (x, y, z) directions and (x_c, y_c, z_c) represent the coordinates for the computed center of mesh. The surface normal vector for each point and the angle between the two neighboring triangles on the mesh (torsion angle) are computed. A set of sharp edge points E can be obtained for all the points on the edges with torsion angle greater than $25°$ as shown in black in Fig. 2 and is described by equation (1) where $\angle(x, y, z)$ is the surface normal difference angle of point (x, y, z).

$$E = \left\{ (x, y, z) | \angle(x, y, z) > 25° \right\} \quad (1)$$

1) Biological Landmarks: The tip of coronoid process ($LM1$), angular process ($LM6$) and incisor ($LM12$) are considered biological landmarks. The coronoid process lies in the postero-superior region of the mandible and the angular process lies in the postero-inferior; hence the regions of interest are restricted accordingly. $LM1$ and $LM6$ project away from the ramus (posteriorly) and have the maximum value of surface normal vector in the x-direction. Similarly, $LM12$ points superiorly and has the maximum value of surface normal vector in the y-direction. $LM6$ and $LM12$ are defined by equations (2) and (3) respectively.

$$LM6 : g = \{(x, y, z)| \arg\max_{x,y,z} x, y < y_c, (x, y, z) \in E\} \quad (2)$$

$$LM12 : lit = \{(x, y, z)| \arg\max_{x,y,z} y, x < x_c, (x, y, z) \in E\} \quad (3)$$

The most prominent point on the tip of the coronoid process ($LM1$) can be detected in the same way as $LM6$, by restricting the region of interest to $y > 1.5y_c$ along the y-axis.

In the same orientation plane, the deepest point on the anterior margin of the lingual foramen ($LM17$) and the deepest point on the posterior margin of the mental foramen ($LM14$) are identified as the points on the ridge surface [8] from the edge candidate point set E in the appropriate restricted regions of interest. $LM3$ and $LM14$ are shown in Fig. 2 as identified by our method.

2) Fuzzy Landmarks: To locate the two points on the condylar surface, the region of interest is restricted as $x > x_{cor}$ along the x-axis and $y > y_c$ along the y-axis. Among the candidate points with the sharp edges on the articular surface of the condyle, the point with the largest y value is selected as the most antero-superior point on the condylar process ($LM3$) and the most posterior point with the minimum y value is idenfied as ($LM4$). The fuzzy landmarks identified using equations (4) and (5) and an example for $LM3$ are shown in Fig. 2.

$$LM3 : cda = \{(x, y, z)| \arg\max_{x,y,z} y, x > x_{cor},$$
$$y > y_c, (x, y, z) \in E\} \quad (4)$$
$$LM4 : cdi = \{(x, y, z)| \arg\min_{x,y,z} y, x > x_{cor},$$
$$y > y_c, (x, y, z) \in E\} \quad (5)$$

Three points on the mental process are identified by clipping the region of interest as $x < x_c$ along the x-axis and $y < y_c$ along the y-axis. The deepest point with the minimum value in the y direction in each cluster is selected as the most prominent postero-inferior point ($LM9$), the most prominent point on middle prominence ($LM10$) and the most prominent antero-inferior point ($LM11$), respectively, moving postero-anteriorly on the medial surface of mandible.

To find the midpoint on alveolar ridge lingual to incisor ($LM13$), the region is restricted to $1.2x_{lit} < x < x_m$ along the x-axis, and the landmark is identified as the furthest posterior point to the incisor when viewed superiorly having the maximum curvature on the ridge surface in the y direction (upwards).

The peak of the curvature from the candidate edge point set E between the region of interest ($LM14$) and ($LM16$) along the x-axis is identified as the masseteric tubercle given by equation (6) such that $H < 0$ & $K > 0$, where H is the
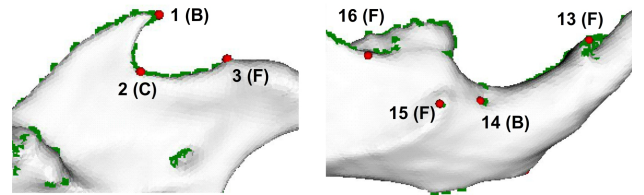

Fig. 2. Automated detection of Type-B (LM1, LM14), Type-C (LM2), and Type-F (LM3, LM13, LM15 and LM16) landmarks (red) selected from identified candidate edge points (green).

Mean curvature and K is the Gaussian curvature [8].

$$LM15 : mtr = \{(x,y,z)| \arg\min_{x,y,z} z, x_{men} < x < x_{urm},$$
$$(x,y,z) \in E\} \quad (6)$$

Following a similar geometric approach, the intersection of the coronoid process and body of mandible is marked as ($LM16$) by finding the minimum curvature point in the region $x > x_{mtr}$ along the x-axis and $y > y_c$ along the y-axis.

3) Constructed Landmarks: To find the deepest point on the sigmoid notch ($LM2$), the region is restricted as $x < x_{cda}$ along the x-axis and $y > y_{cdi}$ along the y-axis, and the point with the minimum value in the y-direction is chosen as ($LM2$). For the landmark on the posterior border of the ramus, the region $x > x_{gn}$ along the x-axis and $y < y_{cdi}$ along the y-axis is extracted and the minimum value in the x-direction is selected as the deepest (anterior) point on the posterior border of the ramus ($LM5$). These are defined by equations (7) and (8). An example of constructed $LM2$ is shown in Fig. 2.

$$LM2 : sgn = \{(x,y,z)| \arg\min_{x,y,z} y, x < x_{cda},$$
$$y > y_{cdi}, (x,y,z) \in E\} \quad (7)$$

$$LM5 : pra = \{(x,y,z)| \arg\min_{x,y,z} y, x > x_{gn},$$
$$y < y_{cdi}, (x,y,z) \in E\} \quad (8)$$

The most prominent point on the middle protrusion of the angular process ($LM7$) is chosen from the candidate points for which the y has the minimum value in the region $x < x_{sgn}$ and $y > y_{pra}$. Similarly, the point having the maximum value in the y direction in the region from $x > x_{gn}$ and $y < y_{iap}$ is the deepest point on the inferior border of the ramus ($LM10$). Both points are selected from the sharp edge point set E and are computed as shown in equations (9) and (10).

$$LM7 : iap = \{(x,y,z)| \arg\min_{x,y,z} y, x < x_{sgn},$$
$$y > y_{pra}, (x,y,z) \in E\} \quad (9)$$

$$LM10 : mpp = \{(x,y,z)| \arg\max_{x,y,z} y, x > x_{gn},$$
$$y < y_{iap}, (x,y,z) \in E\} \quad (10)$$

V. RESULTS AND DISCUSSION

Precision of landmark identification is a measure of repeatability, i.e. the degree to which the landmark is identified at the same place multiple times; while accuracy reflects the truth of the outcome, i.e. whether the landmark is at the correct position. Random human errors are introduced during manual annotation, which results in variability of landmark identification, affecting both precision and accuracy (intra- and inter observer variability respectively). In our study, the overall median intra-investigator variability was ∼0.05 mm, with the greatest error being 0.61 mm (Q1=0.03 mm, Q3=0.09 mm). As expected, the median inter-investigator variability was larger, ∼0.09 mm, with the greatest error measured at 0.85 mm (Q1=0.04 mm, Q3=0.21 mm). These values are similar to those obtain by Tautz *et.al.* [5] who assessed errors in manual annotation of consomic *Mus musculus* mandibles.

Fig.3 is a representative output from our algorithm-based landmark identification, which shows that all points closely match their description and adhere to the definitions (Fig.1, Table I). Our algorithm returns the same output between trials, when repeated on the same specimen and hence shows no variation (and infinite precision). Lacking a *gold-standard* (i.e. error-free set of landmarks), we used manual landmarks to assess accuracy of our algorithm. Landmark positions from the first investigator were considered the *reference set* and errors obtained by our automated method and by another investigator (manual) to this set, were compared. Table II shows these median errors with the first and the third quartiles for each
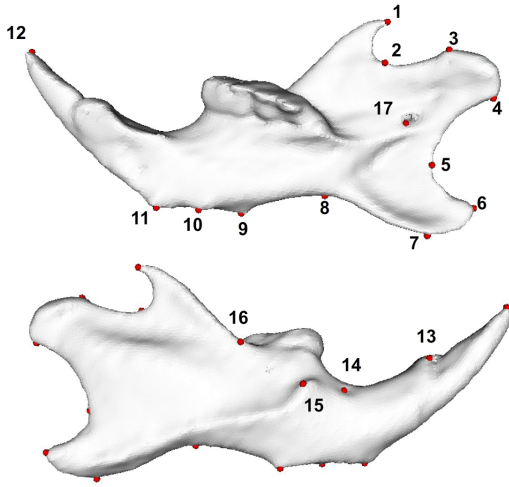

Fig. 3. Representative mandible mesh with 17 automated landmarks (red).

TABLE II
MEDIAN ERRORS WITH Q1 AND Q3 FOR MANUAL AND AUTOMATED
METHODS COMPARED TO THE REFERENCE LANDMARK SET

| LM #	Manual - Ref (mm)			Automated - Ref (mm)			Type
	Median	Q1	Q3	Median	Q1	Q3	
1	0.023	0.013	0.037	0.030	0.019	0.045	B
2	0.138	0.050	0.235	0.233	0.108	0.251	C
3	0.110	0.082	0.227	0.176	0.116	0.394	F
4	0.387	0.275	0.527	0.101	0.064	0.135	F
5	0.066	0.045	0.126	0.077	0.065	0.112	C
6	0.034	0.022	0.056	0.028	0.013	0.043	B
7	0.374	0.292	0.477	0.064	0.053	0.132	C
8	0.441	0.368	0.526	0.214	0.119	0.277	C
9	0.056	0.034	0.079	0.114	0.058	0.179	F
10	0.085	0.041	0.129	0.197	0.158	0.297	F
11	0.043	0.023	0.060	0.099	0.053	0.152	F
12	0.123	0.069	0.206	0.163	0.106	0.196	B
13	0.051	0.031	0.071	0.121	0.072	0.148	F
14	0.072	0.053	0.092	0.121	0.078	0.150	B
15	0.358	0.230	0.599	0.359	0.290	0.496	F
16	0.084	0.042	0.102	0.105	0.072	0.127	F
17	0.049	0.027	0.101	0.049	0.037	0.083	B
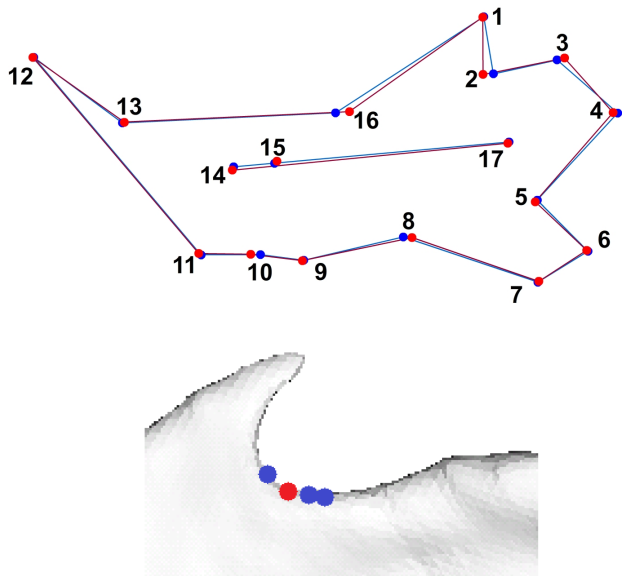
Fig. 4. Superimposition of Procrustes mean coordinates from manual (blue) and automated (red) landmarks obtained from C57BL6/J mandibles (Top). Representative mandible mesh annotated with $LM2$ identified by the algorithm (red) and three investigators (blue, Bottom).
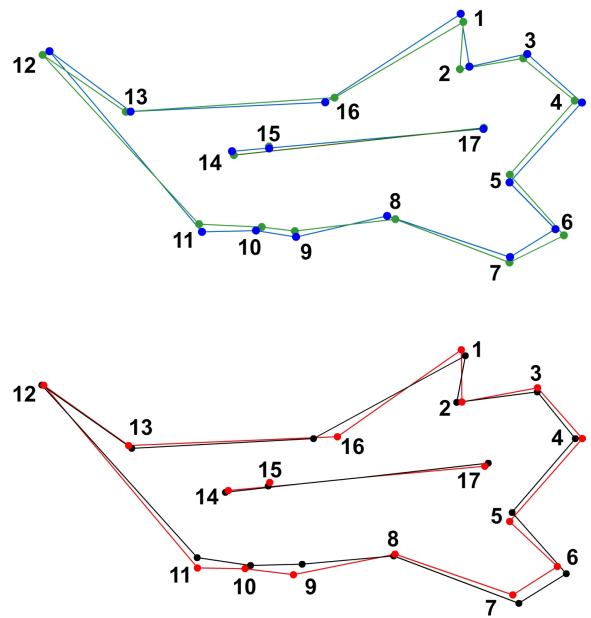

Fig. 5. Shape differences between mandibles from AJ and C57BL/6 strains. Procrustes superimposition of mean coordinates from manual annotation of C57BL/6 (blue) and AJ (green) mandibles (Top), and automated annotation of C57BL/6 (red) and AJ (black) mandibles (Bottom).

landmark. A similar distribution of errors was found with no statistically significant difference between groups [Mann-Whitney U=104384.5, $U\mu$=101250, $U\sigma$=3899.28, Z=0.804, P(one-tailed)=0.421]. We also performed a Procrustes fit of landmarks in each set (i.e. reference, manual and automated) following which co-variance matrices were derived and compared using Morpho J [9]. The co-relation between the co-variance matrices of the manual and reference set was 0.670 while that between the automated and reference set was 0.653 (p-values < 0.0001), suggesting an equivalent degree of shape similarity between the three sets of landmarks. It should be noted that our reliance on manual landmarks to estimate accuracy of the automated method reflects the baseline errors inherent to the manual method. Hence, greater accuracy of the automated method cannot be demonstrated, however, there is clear indication that it is not less accurate than manual annotation.

By definition, landmarks are anatomically relevant points that can be reproducibly recognized. Humans rely on perception and interpretation of anatomic features to aid in this recognition, which as demonstrated, is prone to error. In comparison, the accuracy of the automated method is inherent to the definitions used to construct the algorithm and the mathematical parameters imposed upon landmark selection criteria. A wireframe diagram of the Procrustes mean shape (Fig.4, top) of the reference (blue) and automated (red) sets superimposed at the centroids, shows that most landmarks are very close, with some differences in identification of Type-C landmarks ($LM2$) and Type-F ($LM3$ and $LM16$) landmarks. This is not surprising, since the largest errors in the manual

method are found in Type-C and Type-F landmarks (Table II), in line with earlier reports [7]. Fig.4 (bottom) shows a representative mandible mesh annotated with the Type-C landmark $LM2$ identified by three investigators (blue) as well as our algorithm (red). As can be seen, the location chosen by the algorithm fits the description in Table I closely, while each investigator has some error. Such errors highlight the subjective nature of the manual method, validating the need for an automated method.

Our initial, manually landmarked data also contained a few extreme outliers resulting from swapping of landmarks by one investigator. Another such commonly found systematic error in symmetrical datasets (such as whole skull) is transposition of points across the plane of symmetry. Since these do not constitute random errors, they are not commonly reported in studies (and were not included here), yet they are invariably encountered and can cost investigators significant time and effort to identify and rectify. Such errors are also eliminated if the annotation process is automated.

We also compared the Procrustes mean shapes of mandibles of mice belonging to the C57BL/6 and AJ strains (age and sex matched). The inferred shape differences between these mandibles when analyzed using manual landmark coordinates (Fig.5, top) are similar to using automated landmarks (Fig.5, bottom), i.e., a larger angular process with flattening of the mental process in the AJ mandibles. Discriminate function analysis performed using Procrustes mean coordinates for each strain mis-classifies ~12% mandibles into incorrect groups upon cross-validation, if manually obtained landmarks are used. In contrast, using automated landmarks resulted in the

correct allocation of all mandibles to the appropriate groups upon cross validation, suggesting reduced variability in the data. Additionally, we performed Euclidean Distance Matrix Analysis (EDMA), on the automated and manually obtained landmark sets for the two strains. This analysis computes ratios of all corresponding interlandmark distances in the groups being analyzed, from which shape differences between groups can be localized to anatomical sub-regions. Statistically significant differences in scale and shape between the AJ and C57BL/6 mandibles were identified by both the manual and automated methods. However, the data obtained from the automated method returns a higher number of statistically different ratios compared to the manually annotated sets (data not shown), presumably due to reduction in random errors encountered during manual annotation. Together, these data demonstrate that commonly used shape analyses methods provide statistically superior results when utilizing data from the automated method. This can enhance the power of geometric morphometric studies aimed at analyzing biological variability due to genetic/epigenetic/environmental influences on growth. Furthermore, it has the potential to decrease sample sizes, hence reducing cost associated with sample acquisition. Finally, our automated method has the additional benefit of significantly reducing the labor involved in landmark collection.

Our algorithm can handle moderate anatomical variations, which are typical and expected in studies investigating morphological differences within a species, or closely related species. For example, all landmarks were successfully identified on a mandible of *Acomys cahirinus*, which belongs to the same family as the *Mus musculus* (data not shown). If application to different species or anatomical regions of interest is desired, algorithms would need to be modified or new ones would have to be developed. In contrast, the recently described semi-automated approach [5] can be applied to any 3D structure. However, this method requires the prior creation of a manually annotated training set from which landmark locations on query images are estimated. Hence, their output incorporates the inherent variability in the training set, while our method has no variability (since it follows strict mathematical criteria) except that which occurs naturally (biological variation).

A major limitation of landmark-based geometric morphometrics is the inability to capture or describe shape changes between chosen points. In part, this can be overcome by using semi-landmarks, which represent equally spaced surface points between two established landmarks. Semi-landmarks are typically generated after initial landmark placement and therefore, inherit the variability associated with manual landmarking. Automated landmarking can eliminate this variability and hence improve the efficiency of semi-landmark-based techniques.

VI. Conclusion

The automated landmark detection algorithm presented in this study offers an efficient and arguably superior alternative to the manual method used currently to identify landmarks for geometric morphometric analyses. Our ultimate goal is to establish efficient, versatile and standardized tools for detection of craniofacial landmarks and streamlining downstream analytical applications. Currently, our method requires minimal user input to orient the mandibles in a rough initial configuration; however this process will be facilitated by providing a quick, template based graphical interface in the final application. Additionally, the algorithms presented here will be extended to locate additional landmarks on the mandible as well as other bones of the craniofacial skeleton. Our lab is also working to develop deformable registration based methods to analyze overall shape differences independent of coordinate data. This method relies on initial registration on few established, user-defined landmarks. Applying the methods described here for landmark identification will aid in initial registration, completely automating this process [10].

References

[1] P. Perakis, G. Passalis, T. Theoharis, and I. A. Kakadiaris, "3d facial landmark detection & face registration," *University of Athens, Tech. Rep., January*, 2011.

[2] P. Nair and A. Cavallaro, "3-d face detection, landmark localization, and registration using a point distribution model," *Multimedia, IEEE Transactions on*, vol. 11, no. 4, pp. 611–623, 2009.

[3] S. Liang, J. Wu, S. M. Weinberg, and L. G. Shapiro, "Improved detection of landmarks on 3d human face data," in *Engineering in Medicine and Biology Society (EMBC), 2013 35th Annual International Conference of the IEEE*, pp. 6482–6485, IEEE, 2013.

[4] J. Liu, W. Gao, S. Huang, and W. L. Nowinski, "A model-based, semi-global segmentation approach for automatic 3-d point landmark localization in neuroimages," *Medical Imaging, IEEE Transactions on*, vol. 27, no. 8, pp. 1034–1044, 2008.

[5] P. A. Bromiley, A. C. Schunke, H. Ragheb, N. A. Thacker, and D. Tautz, "Semi-automatic landmark point annotation for geometric morphometrics," *Frontiers in Zoology*, vol. 11, no. 1, p. 61, 2014.

[6] C. J. Valeri, T. M. Cole, S. Lele, and J. T. Richtsmeier, "Capturing data from three-dimensional surfaces using fuzzy landmarks," *American journal of physical anthropology*, vol. 107, no. 1, pp. 113–124, 1998.

[7] F. L. Williams and J. T. Richtsmeier, "Comparison of mandibular landmarks from computed tomography and 3d digitizer data," *Clinical Anatomy*, vol. 16, no. 6, pp. 494–500, 2003.

[8] P. J. Besl and R. C. Jain, "Invariant surface characteristics for 3d object recognition in range images," *Computer vision, graphics, and image processing*, vol. 33, no. 1, pp. 33–80, 1986.

[9] C. P. Klingenberg, "Morphoj: an integrated software package for geometric morphometrics," *Molecular Ecology Resources*, vol. 11, no. 2, pp. 353–357, 2011.

[10] S. Rolfe, E. Camci, E. Mercan, L. Shapiro, and T. Cox, "A new tool for quantifying and characterizing asymmetry in bilaterally paired structures," in *Engineering in Medicine and Biology Society (EMBC), 2013 35th Annual International Conference of the IEEE*, pp. 2364–2367, IEEE, 2013.